

Enhanced removal of doxycycline by iron modified sludge derived hydrothermal biochar: adsorption properties and the effect of Cu(II) coexisting

Xiaohui Liu, Yitao Liu, Jia Wei*, Yuhan Zhu, Yifei Zhang, Luyi Xing, Jun Li

College of Architecture Engineering, Beijing University of Technology, 100 Pingleyuan, Chaoyang district, Beijing 100124, China, Tel. +86-17812020596; emails: weij@bjut.edu.cn (J. Wei), liuxiaohui1996@163.com (X. Liu), yitaoliu2021@163.com (Y. Liu), zhu-yuhan1209@163.com (Y. Zhu), 1442989598@qq.com (Y. Zhang), 1102769502@qq.com (L. Xing), junlihappy2021@163.com (J. Li)

Received 1 November 2020; Accepted 27 April 2021

ABSTRACT

Recently, the use of biochar for wastewater treatment has become a central focus in environmental remediation studies. In this research, a simple and economical one-pot hydrothermal strategy was developed for the synthesis of iron-modified sludge-derived hydrothermal biochar (ISHB). The obtained optimum ISHB possesses abundant hydroxy, carboxyl and aromatic ring surface functional groups as well as relative high surface area and small particle size which contribute to the adsorption of the enhanced contaminants. The structure-activity relationship and the adsorption behavior between the ISHB and doxycycline (DOX) were explored. The loaded iron improved the adsorption capacity of ISHB from 51.65 to 78.93 mg g⁻¹ at 20°C with an initial DOX concentration of 60 mg L⁻¹. As Cu(II) exists in the DOX solution, the adsorption of DOX is inhibited to 50.06 mg g⁻¹ due to the site competition between DOX and Cu(II). Nevertheless, the adsorption of Cu(II) is promoted, which can be explained by the complexation between DOX and Cu(II).

Keywords: Hydrothermal biochar; Sewage sludge; Iron modified; Doxycycline; Cu(II)

1. Introduction

Since penicillin was discovered by Fleming in 1929 and used by Florey and Chain in clinical practice, hundreds of antibiotics have been developed and utilized. By the end of 2017, the annual production of antibiotics in China has been estimated to 210,000 tons, which is two times more than in Europe and the United States [1]. However, the majority of antibiotics are poorly metabolized and thus excreted by excrement and urine of humans and animals [2,3]. When the concentration of antibiotics in the water environment reaches a certain value, it will affect the dynamic balance of the bacterial population and promote the spread of antibiotic resistance. Multidrug resistance of pathogenic bacteria will lead to chronic poisoning, mutagenesis, carcinogenesis and teratogenesis, posing a potential threat to aquatic organisms and humans [4].

From an environmental perspective, removing antibiotics is of great significance, because it is difficult to deal with biological methods. Accordingly, among different removal strategies, adsorption may be the most feasible one on account of its high efficiency, low energy consumption and cost-effectiveness. Several organic and inorganic adsorbents have been tested for the removal of pollutants, such as activated carbon [5], graphene [6] and nanophase materials [7]. For example, the carbon nanotubes were produced by a chemical vapor deposition method and used to remove antibiotics (sulfamethoxazole) from an aqueous solution. The maximum removal capacity for antibiotics could reach 67.9 mg g⁻¹ [8]. However, due to the high manufacturing cost and strict preparation conditions, it was difficult for carbon nanotubes to be widely used in practice. Latterly, biochar has been deemed as a promising adsorbent for pollutants removal owing to

* Corresponding author.

their cheap source (such as crops, poultry droppings and sewage sludge) and straightforward preparation methods (pyrolysis and hydrothermal carbonization methods) [9]. In comparison, the hydrothermal carbonization (HTC) process is more advantageous, which takes place at low temperatures under autogenous pressures in aqueous media and the resulting product possesses a complex pore structure, high specific surface area and a large number of active groups. For instance, *Salix psammophila* was converted via HTC at 300°C and the prepared biochar was applied to tetracycline antibiotic removal with the maximum adsorption capacity of 28.77 mg g⁻¹ [10].

Recently, the production of sewage sludge was from 9 million metric tons in 2005 [11] increased to 34 million metric tons in 2015 [12] (at a moisture content of 80%). A small quantity of sewage sludge (less than 30%) in China [13] has been disposed by conventional ways including composting, land/ocean disposal and incineration, etc. Meanwhile, most of the sewage sludge was not properly disposed which would significantly contribute to secondary pollution in the soil and aquatic environment. Since the excess sludge contains a large amount of biomass and organic matter, it can also be used as a raw material for biochar preparation. For example, sludge-derived biochar was prepared through pyrolysis at 550°C and employed to adsorb 19.80 mg g⁻¹ fluoroquinolone antibiotics [14]. However, the pyrolysis of biochar requires dry raw materials, the high moisture content of sewage sludge would waste a lot of energy in dehydration. Therefore, the sewage sludge is more suitable for hydrothermal treatment. Meanwhile, in order to improve the performance of sludge obtained biochar, iron was used for the biochar modification, because the iron oxides had large surface areas and the capability to adsorb both organic and inorganic materials [15]. However, the application of this modification method to hydrothermal biochar is still relatively rare. Especially, if the iron is loaded on the hydrothermal biochar by a one-step method, the preparation efficiency of the modified biochar will be greatly improved.

Herein, iron-modified sludge-derived hydrothermal biochar (ISHB) was readily prepared via one-step HTC and used to remove antibiotics. Among numerous antibiotics, tetracyclines are the second largest group that are being produced and used annually [16]. Doxycycline (DOX), one of the tetracycline antibiotics, was selected as a model compound due to its high residual toxicity in surface and groundwater [17]. Additionally, some circumstantial evidence have exhibited that the treatment of combined pollution of heavy metals and antibiotics is more difficult than that of traditional contaminants [18]. Cu(II) is among the widespread heavy metal contaminants of the water resources, which is often added to feed as an essential micronutrient to promote animal growth and increase feed utilization. This greatly increases the risk of combined contamination of antibiotics and Cu(II) in the environment. Hence, Cu(II) is chosen as representative of heavy metal ions to study the metal effects on the adsorption of DOX.

The objective of this work was to prepare ISHB through a one-step hydrothermal method and study the adsorption properties of ISHB for the removal of DOX.

The specific objectives were as follows: (1) to explore the existing form of iron and its influence on the change of carbon structure and adsorption properties; (2) elucidate the removal mechanism of DOX by ISHB; (3) investigate the mutual effects of Cu(II) and DOX during the adsorption process.

2. Materials and methods

2.1. Materials

The sewage sludge (moisture content is 99.6%, pH is 6.7) taken from the Gaobeidian Sewage Treatment Plant in China was used as a carbon source for the production of ISHB. Doxycycline hydrochloride (DOX, Molecular Weight: 480.90 g mol⁻¹, C₂₂H₂₄N₂O·HCl, purity ≥ 98%) was purchased from Aladdin Industrial Corporation, USA. The other chemicals including (NH₄)₂Fe(SO₄)₂·6H₂O and CuSO₄·5H₂O were purchased from Tianjin Guangfu Development Company Limited, China. A stock solution of adsorbate (DOX and CuSO₄) was prepared by dissolving its required amounts in 1,000 mL of deionized water. All chemicals were used as purchased without further purification, and all solutions were prepared with high purity deionized water with an electrical conductivity of 2 μS cm⁻¹.

2.2. Methods

2.2.1. Preparation and modification of ISHB

Sludge was centrifuged to lower moisture content (92%) for subsequent HTC experiment, which was conducted in a 1 L high-pressure autoclave equipped with stirrer bar, heater coil, temperature control, water cooling coil and venting valve for gases. The preliminary experiment has proved that hydrothermal temperature 180°C and retention time 3 h were the optimum preparation conditions. The obtained product was separated by centrifugation at 5,000 rpm for 10 min and rinsed several times with distilled water to wipe off the surface residue. Whereafter, it was transferred to a drying oven set at 105°C for 24 h and passed through a 70-mesh nylon sieve. Finally, the fraction containing particles with a size <210 μm was sealed in plastic bags in the dark and stored in a desiccator at room temperature. The ISHB can be prepared in one step by added different amount of (NH₄)₂Fe(SO₄)₂·6H₂O before the hydrothermal process, and other handling methods are the same as above. A mixture containing a certain amount of centrifuged sludge, and 0.00, 12.5, 25.0, 37.5, 50.0 mmol of iron salt ((NH₄)₂Fe(SO₄)₂·6H₂O) was used to fabricate hydrothermal biochar as pristine biochar, 1[#]-ISHB, 2[#]-ISHB, 3[#]-ISHB, 4[#]-ISHB, respectively.

2.2.2. Material characterization

To comprehend the feature of the ISHBs, several characterization studies were performed. The elements of materials were measured using X-ray fluorescence (XRF-1800) (Shimadzu, Japan), equipped with an Rh radiation source. X-ray diffraction (XRD) patterns were recorded using a D8 advance diffractometer, equipped with a Cu Kα radiation source (λ = 1.5418 nm) and an angle from 10° to 80° (BRUKER, Germany). Fourier-transform

infrared spectroscopy (FTIR) was recorded on a Nicolet 6700 (Thermo, USA) spectrometer. Spectra were scanned over the range of 400–4,000 cm^{-1} . The specific surface area and pore size of the product were determined by a Surface Area and Porosity Analyzer (Quantachrome, China) and calculated from N_2 sorption isotherms by the Brunner–Emmet–Teller (BET) method (Sample was degassed at 105°C for 24 h and liquid nitrogen temperature was 77 K).

2.2.3. Adsorption experiment

The pristine biochar and ISHBs were done to investigate the influence of iron loading amount with varying initial DOX concentration. The adsorption of DOX was determined using triplicate batch tests, and 40 mL standard sample vials with Teflon-lined septa and screw caps were utilized. After 24 h, the solutions were centrifuged for 20 min by the centrifuge with a 5,000 rpm rotation speed. A small amount of supernatant (15–20 mL) was taken out after centrifugation and diluted a certain multiple. The DOX concentration was determined eventually by a 765 UV-vis spectrophotometer with the absorbance being measured at $\lambda = 346$ nm in cuvettes. The product with the best adsorption capacity was selected and applied to the subsequent adsorption experiment.

The adsorption isotherm and thermodynamics experiments were conducted in a constant temperature shaker (200 rpm) at three temperatures (20°C, 30°C, and 40°C) with different initial DOX concentrations. Adsorption kinetics experiments were conducted at 20°C with an initial DOX concentration of 60 mg L^{-1} and an adsorbent dosage of 0.6 g L^{-1} . The antibiotic concentrations at different time intervals were determined until equilibration.

To evaluate the effect of the Cu(II) existence on DOX adsorption, the binary adsorption experiments were conducted by varying DOX or Cu(II) concentration with another one kept constant at 20°C. As adsorption reached equilibrium, the concentration of Cu(II) was determined by a ZA3300 flame atomic absorption spectrometer.

The amount of contaminant adsorbed to the ISHB was calculated by deducting the mass remaining in the aqueous phase at equilibrium from the initial mass spiked into the aqueous phase. The adsorption capacity is calculated by Eq. (1):

$$Q_t = \frac{V(C_0 - C_t)}{m} \quad (1)$$

where V (L) is the solution volume; C_0 (mg L^{-1}) and C_t (mg L^{-1}) denote the concentrations of the contaminant at the start and at time t , respectively; m (g) is the adsorbent mass; Q_t (mg g^{-1}) is the amount of contaminant adsorbed on the adsorbent at time t .

3. Results and discussion

3.1. Characteristics of ISHB

The results of XRF showed that the iron content of pristine biochar, 1[#]-ISHB, 2[#]-ISHB, 3[#]-ISHB and 4[#]-ISHB is 3.87%, 9.32%, 11.94%, 12.94% and 13.64%, respectively.

The iron in pristine biochar may be derived from the addition of ferrous sulfate coagulant in the sewage treatment process. With the increase in the amount of iron salt added, the iron constituent in ISHB continues to increase, which proves that iron is indeed loaded.

Fig. 1 presents the XRD patterns of pristine biochar and all ISHB samples. All of the data were analyzed by Jade 5.0 according to different standard cards comparison. The wide peak at 19.887° represents amorphous carbon and the peak at 26.624° is graphite crystal [19]. The content of graphite decreases slightly with increasing the amount of iron-loaded. The XRD patterns for 1[#]-ISHB and 2[#]-ISHB samples show peaks for FeOOH at angles of 26.725°, 35.161° and 39.219° [20,21] and FeO at angles of 36.283°, 41.169° [22]. With the increase of loading iron amount, the crystal shape of the loaded iron had been changed. The patterns for 3[#]-ISHB and 4[#]-ISHB samples show peaks for FeOOH at angles of 21.223°, 36.649° but no peaks for FeO. The size of the pristine biochar and ISHBs are 77.2 nm (pristine biochar), 56.4 nm (1[#]-ISHB), 31.2 nm (2[#]-ISHB), 59.2 nm (3[#]-ISHB) and 81.0 nm (4[#]-ISHB), proving loaded iron may change the particle size. When a little amount of iron salt is added, Fe^{3+} and Fe^{2+} can load on the biomass and conjunct with the sludge during the HTC process. The conjunct iron ion can be seen as the “separation agent”, which would “cut” the biochar particles into many minces in a small area [23]. While, as the iron salt amount increase, ferumoxytol is liable to agglomerate [24] causing the increase of grain size.

FTIR analysis presents typical structural properties of obtained samples (Fig. 2). The peaks at 1,077 and 3,420 cm^{-1} belong to the O–H [25] bond indicating that ISHBs remain with a significant number of –OH groups on its surface. The peaks at 2,855 and 2,933 cm^{-1} are stretching vibration of C–H for – CH_3 and – OCH_3 in aliphatic hydrocarbons, respectively. The peaks of ISHBs at 1,642 and 1,459 cm^{-1} are assigned to carboxylate groups and C=C bonds [26] in aromatic compounds which are slightly more prominent compared to that in pristine biochar spectrum. This could be due to an increase in aromaticity and the amount of oxygen-containing

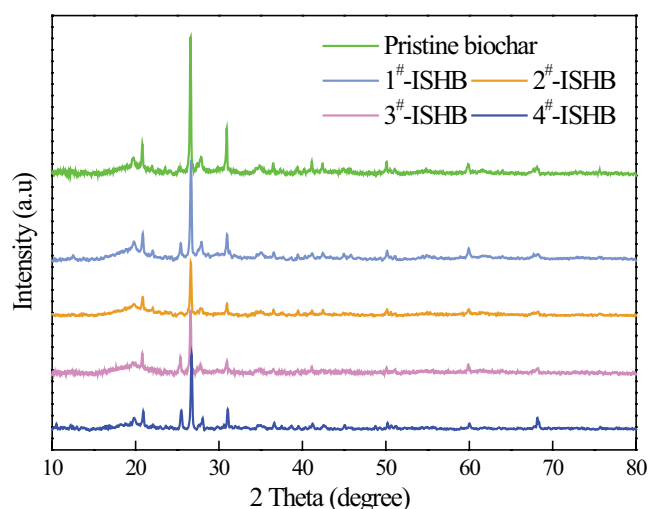


Fig. 1. X-ray patterns of the pristine biochar and ISHB samples.

functional groups in the modified sample. For all samples, the main surface functional groups are similar but their intensities show a slight difference, implying that modification does not change the types of functional groups but changes their contents. The significantly enhanced band of ISHBs at 554 cm^{-1} may be attributed to Fe–O stretching bond [27].

Table 1 lists the surface and porous characteristics of as-prepared samples. According to the pore diameter, all of ISHBs are presented as microporous structures (pore diameter $< 2\text{ nm}$). However, there are high surface areas by the ISHBs, especially 2[#]-ISHB. Meanwhile, the total pore volume of all ISHBs is larger than that of the pristine biochar. It is implied that iron is the key factor to control the morphology of biochar and resulting in the equivalent specific surface area of the ISHB to that of pristine one.

3.2. Adsorption of DOX on ISHB

3.2.1. Effect of the loaded iron amount on DOX adsorption

It is clearly seen from Fig. 3 that the adsorption quantity of DOX is growing gradually with an increase of the added antibiotic concentration from $10\text{ to }60\text{ mg L}^{-1}$, providing an improvement of driving force for the combination of the DOX and the adsorption sites. Especially, the adsorption capacity of ISHB is significantly increased compared with the pristine

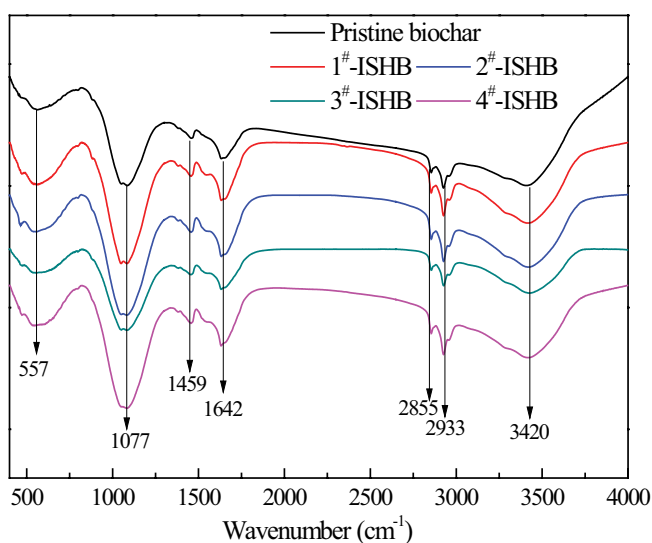


Fig. 2. FTIR images of the pristine biochar and ISHB samples.

Table 1
 S_{BET} characteristics of the pristine biochar and ISHB

Samples	Surface area ($\text{m}^2\text{ g}^{-1}$)	Pore volume ($\text{m}^3\text{ g}^{-1}$)	Pore diameter (nm)
Pristine biochar	70.45	0.379	1.424
1 [#] -ISHB	81.61	0.453	1.413
2 [#] -ISHB	82.78	0.487	1.434
3 [#] -ISHB	74.87	0.447	1.418
4 [#] -ISHB	71.20	0.445	1.416

biochar, and the adsorption effect of 2[#]-ISHB is the best. The results indicate that the amount of iron in biochar fabrication can regulate the adsorptive ability of ISHB obtained. According to the results of FTIR, ISHB has larger amounts of oxygen-containing functional groups than the pristine biochar which can facilitate the chemical adsorption significantly [28]. Moreover, based on the BET and XRD analysis, 2[#]-ISHB has the largest specific surface area and the smallest particle size, leading to the outstanding adsorption effect.

3.2.2. Sorption isotherm studies of ISHB

A successful representation of the dynamic adsorptive separation of solute from a solution onto an adsorbent is dependent upon a good description of the equilibrium separation between two phases. In this study, Langmuir [29] (ideal adsorption model) and Freundlich [30] (empirical models) isothermal models are employed for fitting the experimental data nonlinearly as illustrated in Fig. 4a and b. The model simulation parameters are listed in Table 2.

The adsorption is significantly affected by varying the temperature from 20°C to 40°C . The adsorption capacity increases as temperature increases. The maximum adsorption capacity can be achieved by 289.65 mg g^{-1} . However, the value of Langmuir constant K_L diminishes as the temperature increases, which is due to the fact that the constant K_L is dependent on the temperature and not on the covering of the surface. Whereas, the adsorbed quantity (q_m) on the surface depends on the non-homogeneous nature of the surface [31]. The Freundlich model assumes that there is an exponential variation in site energies of adsorbent, and surface adsorption is not a rate-limiting step. By comparing R^2 , the adsorption process can be described slightly better by the Langmuir model than Freundlich.

3.2.3. Thermodynamic analysis

Here, three thermodynamic parameters, ΔH , ΔS and ΔG are investigated to explore the adsorption of DOX on ISHB (Table 3), respectively.

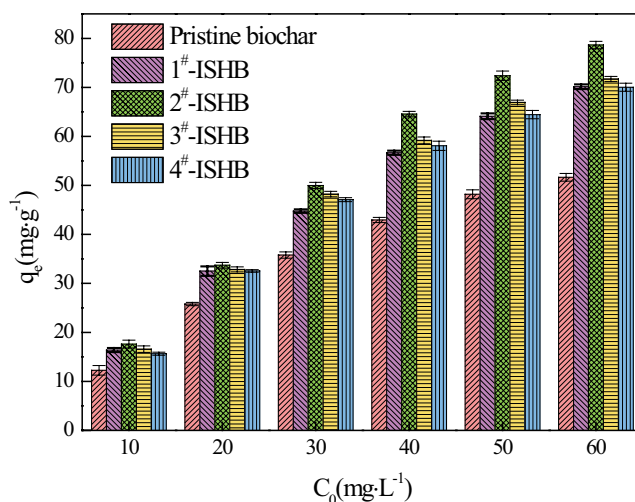


Fig. 3. Effect of loaded iron on the hydrothermal biochar in different initial DOX concentrations.

The negative values of ΔG at different temperatures prove that the adsorption process is feasible and spontaneous. Generally, values of ΔG around -20 kJ mol^{-1} or lower are consistent with the electrostatic interaction between the charged molecules and the charged metal (physisorption). Those more negative than -40 kJ mol^{-1} involve charge sharing or transfer from the inhibitor molecules to the metal surface to form a coordinate type of bond (chemisorption) [32]. The calculated values of ΔG are

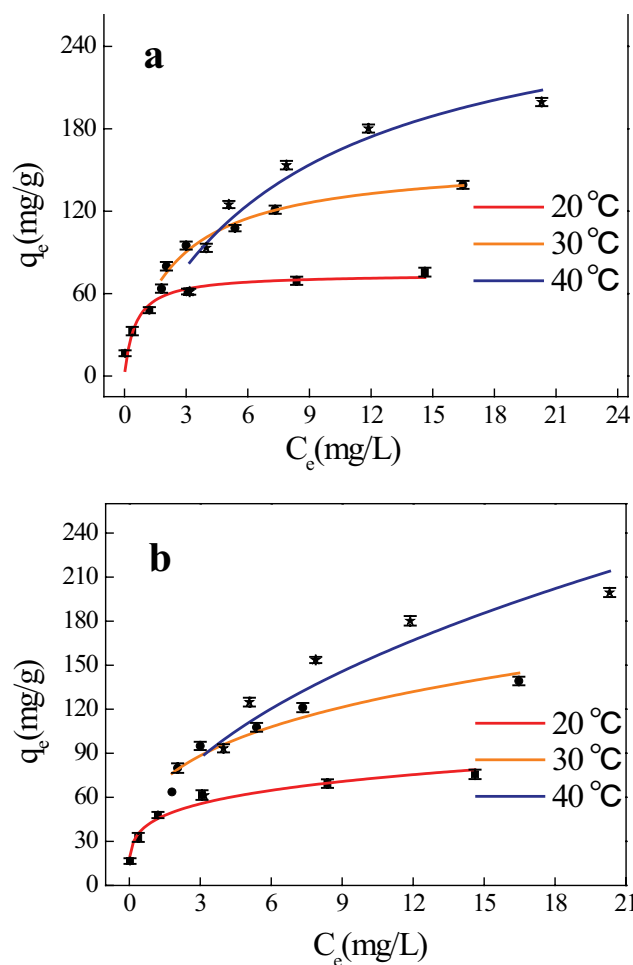


Fig. 4. Adsorption isotherm fittings for DOX (a) Langmuir isotherm and (b) Freundlich isotherm.

Table 2
Isothermal models and fitting parameters of DOX

Models	Expression	Parameters	Temperature (°C)		
			20	30	40
Langmuir	$q_e = \frac{q_m K_L C_e}{1 + K_L C_e}$	R^2	0.9256	0.9663	0.9263
		K_L	1.9179	0.4478	0.1258
		$q_m \text{ (mg g}^{-1}\text{)}$	74.32	157.6	289.6
Freundlich	$q_e = K_F C_e^{1/n}$	R^2	0.9073	0.9054	0.8484
		K_F	43.62	54.29	61.64
		n	4.536	3.455	2.118

almost slightly less negative than -40 kJ mol^{-1} , indicating that the adsorption of DOX on ISHB may be a combination of both physisorption and chemisorption (comprehensive adsorption) [33].

The absolute value of ΔH is higher than 40 kJ mol^{-1} elucidates that chemical adsorption is dominating in the process. Moreover, ΔH is calculated as a negative value which demonstrates that the adsorption process is an exothermic reaction, nevertheless, the adsorption amount of DOX increases with the increasing temperature. This result is consistent with the reports of Zarrouk et al. [34], Brigante and Avena [35] and Lou et al. [36]. Due to the large size of the DOX molecules, great barriers are required to spread across the pores of the bio-char, which require pretty high energy. Compared with low temperature, the external environment can provide more energy at high temperature, and DOX molecules can diffuse more easily. Therefore, although the adsorption reaction is exothermic, the adsorption capacity increases with the increase of temperature.

From the above thermodynamic parameters, it is assured that DOX adsorption on the selected ISHB is composite adsorption (both physical and chemical adsorption). Chemical adsorption is the main process, including hydrogen bonding, π - π electron donor-acceptor (EDA) interactions and complexation. ISHB bears a large amount of oxygen-containing functional groups which can form hydrogen bonds with hydroxyl and amino of DOX. The π - π EDA interactions would emerge between aromatic rings of ISHB and benzene rings of DOX. Additionally, ISHB can form complex with DOX [37].

3.2.4. Adsorption kinetics by ISHB

To gain insight into the adsorption mechanism of DOX on ISHB, several adsorption kinetic models are

Table 3
Thermodynamic parameters of DOX

$T \text{ (K)}$	$\ln K_d$	$\Delta G \text{ (kJ mol}^{-1}\text{)}$	$\Delta H \text{ (kJ mol}^{-1}\text{)}$	$\Delta S \text{ (J (mol K}^{-1}\text{))}$
293.15	14.47	-35.26	-104.0	-234.6
303.15	13.01	-32.80		
313.15	11.74	-30.57		

widely selected to determine the relationship between the amount of adsorbate and the reaction time, fitting the experimental data obtained under the laboratory conditions. Pseudo-first-order kinetic model (Fig. 5a),

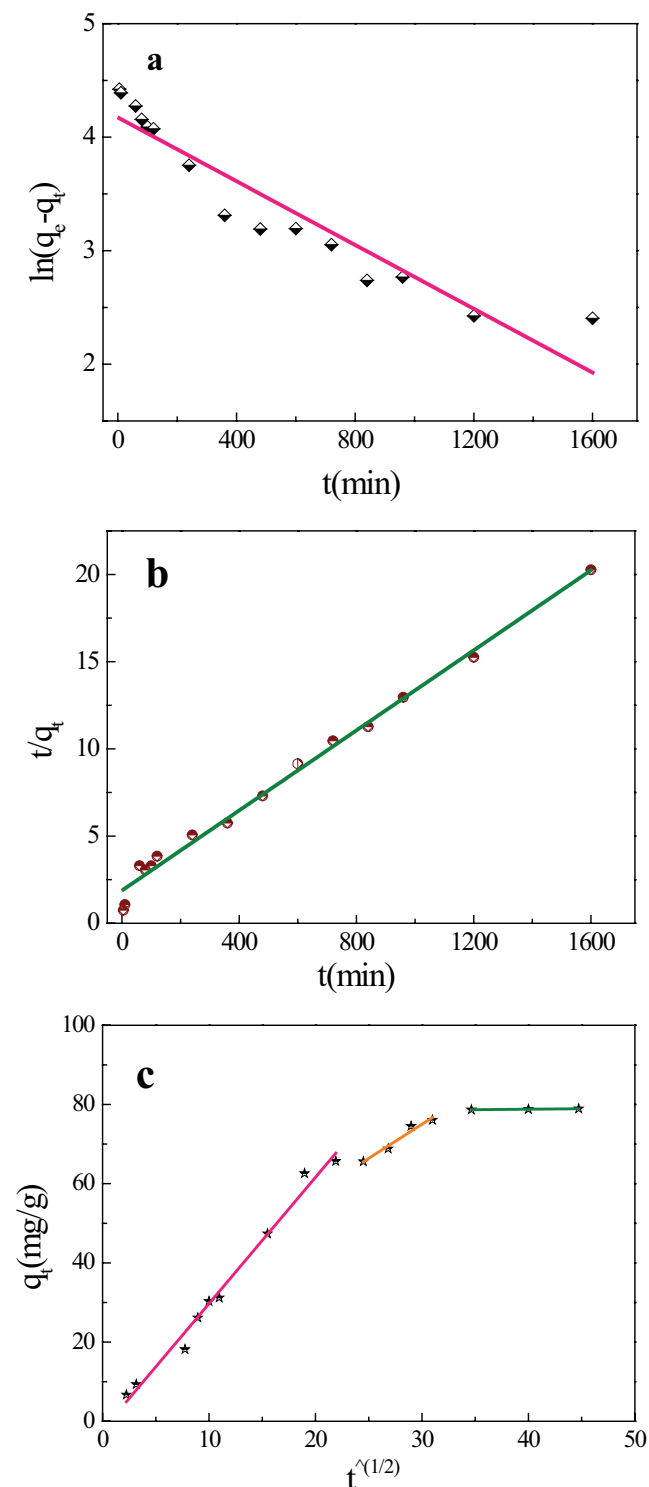


Fig. 5. Adsorption kinetic fittings for DOX (a) pseudo-first-order kinetic, (b) pseudo-second-order kinetic and (c) intraparticle diffusion kinetic.

pseudo-second-order kinetic model (Fig. 5b) and intraparticle diffusion kinetic model (Fig. 5c) are exploited respectively. The kinetic models and calculated parameters are summarized in Table 4.

It is manifested that the correlation coefficient R^2 of the pseudo-second-order kinetic model is higher than that of the pseudo-first-order kinetic model and close to 1. Therefore, it is considered that the pseudo-second-order kinetic model accurately describes the adsorption process of DOX on the ISHB. Furthermore, the intraparticle diffusion model is used to investigate the rate-controlling steps of DOX sorption on ISHB. From the plots of Q_t vs. $t^{1/2}$ of DOX (Fig. 5c), a multi-linearity is observed, denoting the adsorption process is controlled by a multistep mechanism. Firstly, as time goes on, the line rises up sharply. This stage is film diffusion indicating that DOX molecules are transported from the liquid phase to the external surface of the adsorbent through a hydrodynamic boundary layer. Compared with other adsorbents in previous studies [38,39], adsorption of DOX takes a longer time in the first stage. This may explain that the antibiotic molecules are large, requiring more time and energy to transfer from the liquid phase to the adsorbent surface. And then the line keeps a gentle upward tendency which is attributed to the diffusion of the DOX molecules from the exterior of the adsorbent into the pores of the ISHB, known as intraparticle diffusion. At this point, the adsorption on the external surface reaches saturation and the diffusion resistance increases leading to the decrease of diffusion rate. The final stage is the equilibrium step. In the intraparticle diffusion formula, K_p ($\text{mg g}^{-1} \text{min}^{1/2}$) is the rate constant of the model. P (mg g^{-1}) is a constant associated with the thickness of the boundary layer, where a higher value of P corresponds to a greater effect on the limiting boundary layer [40]. Combining calculation parameters, it is clear that as the time is extended, the adsorption rate gradually slows down with the shrinking K_p values, and the increase in P values provides that the resistance of the boundary layer is getting bigger and bigger.

3.3. Effects of Cu(II) coexistence on DOX adsorption

To evaluate the effect of Cu(II) coexistence on DOX adsorption onto ISHB, the binary adsorption experiments were conducted at 20°C by varying concentrations of DOX or Cu(II) with another one fixed. On one hand, it can be seen clearly from Fig. 6 that the addition of DOX promotes the adsorption of Cu(II). Except for the adsorption of Cu(II) itself, the antibiotic can act as a bridge in the formation of complex among Cu(II), DOX and adsorbent, which is ascribed that DOX can be adsorbed on the selected ISHB and its oxygen-containing functional groups can complex Cu(II) [41,42]. When the concentration of DOX is elevated to 100 mg L^{-1} , the adsorption capacity for Cu(II) begins to decline, demonstrating that only a part of Cu(II) form a complex with DOX. While the rest Cu(II) is apt to compete with DOX for negative charge (physical adsorption site), thus reducing the amount of adsorbed Cu(II). On the other hand, the existence of Cu(II) can inhibit the adsorption of DOX by ISHB. This is owing to that the existence of Cu(II) competes with DOX for the site

Table 4
Kinetic models and fitting parameters of DOX

Models	Equation	$k_1 \times 10^{-3}$	R_1^2		
Pseudo-first-order kinetic	$\ln(q_e - q_t) = \ln q_e - k_1 t$	1.4	0.8922		
Pseudo-second-order kinetic	$\frac{t}{q_t} = \frac{1}{k_2 q_e^2} + \frac{t}{q_e}$	$k_2 \times 10^{-5}$	R_2^2		
	$q_t = K_p t^{1/2} + C$	7.016	0.9902		
Intraparticle diffusion kinetic		t (min)	K_p	P	R^2
		0–480	3.19	0.0429	0.9848
		480–960	1.72	23.34	0.9464
		960–2,000	0.024	77.84	0.9729

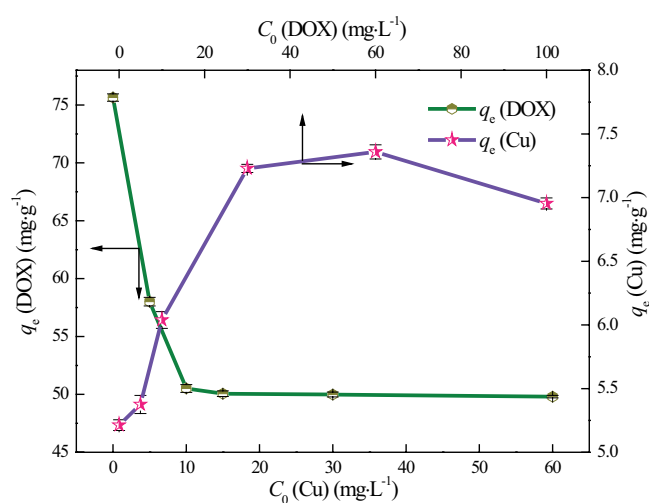


Fig. 6. The DOX (60 mg L^{-1}) adsorption with Cu(II) addition ($0\text{--}60 \text{ mg L}^{-1}$) and the Cu(II) (30 mg L^{-1}) adsorption with DOX addition ($0\text{--}100 \text{ mg L}^{-1}$).

of the adsorption point, accordingly inhibiting the physical adsorption of DOX on ISHB. In general, the inhibitory effect of Cu(II) on the physical adsorption of DOX is far greater than the chemical interaction of Cu(II) and DOX. In other words, Cu(II) has a promoting and suppressing effect simultaneously on the adsorption of DOX on ISHB. However, its promoting effect seemed feeble, so that the adsorption of DOX is reduced. When the Cu(II) concentration increases to 15 mg L^{-1} , the physical adsorption sites on the adsorbent surface are almost occupied by Cu(II) and the adsorption of DOX is only chemisorption. Therefore, the concentration of Cu(II) continues to increase, and its inhibition on DOX is not enhanced dramatically.

4. Conclusions

In this research, a polyporous ISHB, which has a high surface area and abundant surface organic functional groups, was successfully synthesized using the facile one-step hydrothermal method. During the HTC process, the loaded iron ion has a “separation” effect on the carbonization of sludge, resulting in the decrease of biochar particle size and the increase of its specific surface

area. Moreover, it could be inferred that the behavior of DOX and ISHB in aqueous is dominated by chemical interaction. As Cu(II) and DOX coexist in a solution, Cu(II) has suppressing effects on the adsorption of DOX through physical interaction, while DOX promotes Cu(II) adsorption by chemical interaction.

Acknowledgments

The authors would like to acknowledge the financial support by the Beijing Municipal Natural Science Foundation (8202007) and the National Natural Science Foundation of China (51778015).

References

- [1] S. Li, Q. Yang, Y. Ye, Preparation of activated carbon from herbal residues and kinetics of cephalosporin antibiotic adsorption in wastewater, *BioResources*, 12 (2017) 2768–2779.
- [2] A. Hartmann, A.C. Alder, T. Koller, R.M. Widmer, Identification of fluoroquinolone antibiotics as the main source of *umuC* genotoxicity in native hospital wastewater, *Environ. Toxicol. Chem.*, 17 (1998) 377–382.
- [3] C.-H. Huang, J.E. Renew, K.L. Smeby, K. Pinkston, D.L. Sedlak, Assessment of potential antibiotic contaminants in water and preliminary occurrence analysis, *J. Contemp. Water Res. Educ.*, 120 (2001) 30–40.
- [4] A. Pruden, R. Pei, H. Storteboom, K.H. Carlson, Antibiotic resistance genes as emerging contaminants: studies in Northern Colorado, *Environ. Sci. Technol.*, 40 (2006) 7445–7450.
- [5] K. Björklund, L.Y. Li, Adsorption of organic stormwater pollutants onto activated carbon from sewage sludge, *J. Environ. Manage.*, 197 (2017) 490–497.
- [6] A. Sheikmohammadi, S.M. Mohseni, R. Khodadadi, M. Sardar, M. Abtahi, S. Mahdavi, H. Keramati, Z. Dahaghin, S. Rezaei, M. Almasian, M. Sarkhosh, M. Faraji, S. Nazari, Application of graphene oxide modified with 8-hydroxyquinoline for the adsorption of Cr(VI) from wastewater: optimization, kinetic, thermodynamic and equilibrium studies, *J. Mol. Liq.*, 233 (2017) 75–88.
- [7] N.-C. Zheng, Z. Wang, J.-Y. Long, L.-J. Kong, D.-Y. Chen, Z.-Q. Liu, Shape-dependent adsorption of CeO₂ nanostructures for superior organic dye removal, *J. Colloid Interface Sci.*, 525 (2018) 225–233.
- [8] Y. Tian, B. Gao, V.L. Morales, H. Chen, Y. Wang, H. Li, Removal of sulfamethoxazole and sulfapyridine by carbon nanotubes in fixed-bed columns, *Chemosphere*, 90 (2013) 2597–2605.
- [9] J. Liang, X.M. Li, Z.G. Yu, G.M. Zeng, Y. Luo, L.B. Jiang, Z.X. Yang, Y.Y. Qian, H.P. Wu, Amorphous MnO₂ modified biochar derived from aerobically composted swine manure for

- adsorption of Pb(II) and Cd(II), *ACS Sustainable Chem. Eng.*, 5 (2017) 5049–5058.
- [10] J.S. Cha, S.H. Park, S.-C. Jung, C. Ryu, J.-K. Jeon, M.-C. Shin, Y.-K. Park, Production and utilization of biochar: a review, *J. Ind. Eng. Chem.*, 40 (2016) 1–15.
- [11] X. Zhu, Y. Liu, C. Zhou, G. Luo, S. Zhang, J. Chen, A novel porous carbon derived from hydrothermal carbon for efficient adsorption of tetracycline, *Carbon*, 77 (2014) 627–636.
- [12] P.J. He, F. Lü, H. Zhang, L.M. Shao, D.J. Lee, Sewage sludge in China: challenges toward a sustainable future, *Water Pract. Technol.*, 2 (2007) 19–22, doi: 10.2166/wpt.2007.083.
- [13] L. Feng, J. Luo, Y. Chen, Dilemma of sewage sludge treatment and disposal in China, *Environ. Sci. Technol.*, 49 (2015) 4781–4782.
- [14] G. Zhen, X. Lu, Y.-Y. Li, Y. Zhao, Combined electrical-alkali pretreatment to increase the anaerobic hydrolysis rate of waste activated sludge during anaerobic digestion, *Appl. Energy*, 128 (2014) 93–102.
- [15] H. Yao, J. Lu, J. Wu, Z. Lu, P.C. Wilson, Y. Shen, Adsorption of fluoroquinolone antibiotics by wastewater sludge biochar: role of the sludge source, *Water Air Soil Pollut.*, 224 (2013) 1370, doi: 10.1007/s11270-012-1370-7.
- [16] C. Li, D. Jia, Adsorption of 2-naphthalenesulfonic acid/sulfuric acid/sulfurous acid from aqueous solution by iron-impregnated weakly basic resin: equilibrium and model, *Chin. J. Chem. Eng.*, 24 (2016) 1522–1526.
- [17] J. Liang, Y.L. Fang, Y. Luo, G.M. Zeng, J.Q. Deng, X.F. Tan, N. Tang, X.M. Li, X.Y. He, C.T. Feng, S.J. Ye, Magnetic nanoferromanganese oxides modified biochar derived from pine sawdust for adsorption of tetracycline hydrochloride, *Environ. Sci. Pollut. Res.*, 26 (2019) 5892–5903.
- [18] S. Zaidi, T. Chaabane, V. Sivasankar, A. Darchen, R. Maachi, T.A.M. Msagati, M. Prabhakaran, Performance efficiency of electro-coagulation coupled electro-flotation process (EC-EF) versus adsorption process in doxycycline removal from aqueous solutions, *Process Saf. Environ. Prot.*, 102 (2016) 450–461.
- [19] D.W. Graham, S. Olivares-Rieumont, C.W. Knapp, L. Lima, D. Werner, E. Bowen, Antibiotic resistance gene abundances associated with waste discharges to the Almendares River near Havana, Cuba, *Environ. Sci. Technol.*, 45 (2010) 418–424.
- [20] B.T. Hang, I. Watanabe, T. Doi, S. Okada, J.-I. Yamaki, Electrochemical properties of nano-sized Fe₂O₃-loaded carbon as a lithium battery anode, *J. Power Sources*, 161 (2006) 1281–1287.
- [21] H. Liu, Z. Hu, H. Liu, H. Xie, S. Lu, Q. Wang, J. Zhang, Adsorption of amoxicillin by Mn-impregnated activated carbons: performance and mechanisms, *RSC Adv.*, 6 (2016) 11454–11460.
- [22] F. Xiao, W. Li, L. Fang, D. Wang, Synthesis of akaganeite (beta-FeOOH)/reduced graphene oxide nanocomposites for oxidative decomposition of 2-chlorophenol by Fenton-like reaction, *J. Hazard. Mater.*, 308 (2016) 11–20.
- [23] B. Leszczyński, G.C. Hadjipanayis, A.A. El-Gendy, K. Załęski, Z. Śniadecki, A. Musiał, M. Jarek, S. Jurga, A. Skumiel, The influence of oxidation process on exchange bias in egg-shaped FeO/Fe₃O₄ core/shell nanoparticles, *J. Magn. Magn. Mater.*, 416 (2016) 269–274.
- [24] L. Peng, Y. Ren, J. Gu, P. Qin, Q. Zeng, J. Shao, M. Lei, L. Chai, Iron improving bio-char derived from microalgae on removal of tetracycline from aqueous system, *Environ. Sci. Pollut. Res.*, 21 (2014) 7631–7640.
- [25] C. Stauch, S. Späth, T. Ballweg, R. Luxenhofer, K. Mandel, Nanostructured micro-raspberries from superparamagnetic iron oxide nanoparticles: studying agglomeration degree and redispersibility of nanoparticulate powders via magnetisation measurements, *J. Colloid Interface Sci.*, 505 (2017) 605–614.
- [26] B. Kayan, A. Khataee, D. Kalderis, S. Akay, M. Konsolakis, Ultrasound-assisted removal of Acid Red 17 using nanosized Fe₃O₄-loaded coffee waste hydrochar, *Ultrason. Sonochem.*, 35 (2017) 72–80.
- [27] T.C. Nguyen, P. Loganathan, T.V. Nguyen, S. Vigneswaran, J. Kandasamy, R. Naidu, Simultaneous adsorption of Cd, Cr, Cu, Pb, and Zn by an iron-coated Australian zeolite in batch and fixed-bed column studies, *Chem. Eng. J.*, 270 (2015) 393–404.
- [28] L. Wang, N.T. Nguyen, Y. Zhang, Y. Bi, P. Schmuki, Enhanced Solar water splitting by swift charge separation in Au/FeOOH sandwiched single-crystalline Fe₂O₃ nanoflake photoelectrodes, *ChemSusChem*, 10 (2017) 2720–2727.
- [29] Q. Fan, J. Sun, L. Chu, L. Cui, G. Quan, J. Yan, Q. Hussain, M. Iqbal, Effects of chemical oxidation on surface oxygen-containing functional groups and adsorption behavior of biochar, *Chemosphere*, 207 (2018) 33–40.
- [30] I. Langmuir, The constitution and fundamental properties of solids and liquids. II. Liquids, *J. Am. Chem. Soc.*, 184 (1916) 102–105.
- [31] H. Freundlich, Über die Adsorption in Lösungen (over the adsorption in solution) *Zeitschrift für physikalische Chemie*, *J. Am. Chem. Soc.*, 62 (1906) 121–125.
- [32] E.A. Ferreiro, S.G. de Bussetti, Thermodynamic parameters of adsorption of 1,10-phenanthroline and 2,2'-bipyridyl on hematite, kaolinite and montmorillonites, *Colloids Surf., A*, 301 (2007) 117–128.
- [33] C.P. Jordão, R.B.A. Fernandes, K. de Lima Ribeiro, B. de Souza Nascimento, P.M. de Barros, Zn(II) adsorption from synthetic solution and kaolin wastewater onto vermicompost, *J. Hazard. Mater.*, 162 (2009) 804–811.
- [34] A. Zarrouk, B. Hammouti, H. Zarrok, S.S. Al-Deyab, M. Messali, Temperature effect, activation energies and thermodynamic adsorption studies of L-Cysteine methyl ester hydrochloride as copper corrosion inhibitor in nitric acid 2M, *Int. J. Electrochem. Sci.*, 6 (2011) 6261–6274.
- [35] M. Brigante, M. Avena, Biotemplated synthesis of mesoporous silica for doxycycline removal. Effect of pH, temperature, ionic strength and Ca²⁺ concentration on the adsorption behaviour, *Microporous Mesoporous Mater.*, 225 (2016) 534–542.
- [36] Y. Lou, Z. Ye, S. Chen, X. Ye, Y. Deng, J. Zhang, Sorption behavior of tetracyclines on suspended organic matters originating from swine wastewater, *J. Environ. Sci.*, 65 (2018) 144–152.
- [37] E.A. Noor, A.H.A. Moubaraki, Thermodynamic study of metal corrosion and inhibitor adsorption processes in mild steel/1-methyl-4[4'-(X)-styryl pyridinium iodides/hydrochloric acid systems, *Mater. Chem. Phys.*, 110 (2008) 145–154.
- [38] S. Liu, W.-H. Xu, Y.-G. Liu, X.-F. Tan, G.-M. Zeng, X. Li, J. Liang, Z. Zhou, Z.-L. Yan, X.-X. Cai, Facile synthesis of Cu(II) impregnated biochar with enhanced adsorption activity for the removal of doxycycline hydrochloride from water, *Sci. Total Environ.*, 592 (2017) 546–553.
- [39] M. ShahinoorIslam, K.N. McPhedran, S.A. Messele, Y. Liu, M.G. El-Din, Isotherm and kinetic studies on adsorption of oil sands process-affected water organic compounds using granular activated carbon, *Chemosphere*, 202 (2018) 716–725.
- [40] L. Sun, D. Chen, S. Wan, Z. Yu, Performance, kinetics, and equilibrium of methylene blue adsorption on biochar derived from eucalyptus saw dust modified with citric, tartaric, and acetic acids, *Bioresour. Technol.*, 198 (2015) 300–308.
- [41] Z. Tian, B. Yang, G. Cui, L. Zhang, Y. Guo, S. Yan, Synthesis of poly(*m*-phenylenediamine)/iron oxide/acid oxidized multi-wall carbon nanotubes for removal of hexavalent chromium, *RSC Adv.*, 5 (2015) 2266–2275.
- [42] B. Huang, Y. Liu, B. Li, S. Liu, G. Zeng, Z. Zeng, X. Wang, Q. Ning, B. Zheng, C. Yang, Effect of Cu(II) ions on the enhancement of tetracycline adsorption by Fe₃O₄@SiO₂-Chitosan/graphene oxide nanocomposite, *Carbohydr. Polym.*, 157 (2017) 576–585.
- [43] W. Xu, H. Lan, H. Wang, H. Liu, J. Qu, Comparing the adsorption behaviors of Cd, Cu and Pb from water onto Fe-Mn binary oxide, MnO₂ and FeOOH, *Front. Environ. Sci. Eng.*, 9 (2015) 385–393.